Energy and Buildings 118 (2016) 1–17

Contents lists available at ScienceDirect

Energy and Buildings

journal homepage: www.elsevier.com/locate/enbuild

Development of annual daylight simulation algorithms for prediction of indoor daylight illuminance

Younju Yoon [a], Jin Woo Moon [b], Sooyoung Kim [c,*]

[a] Samsung C&T Corporation, Construction Technology Center, Seoul, South Korea
[b] School of Architecture and Building Science, Chung-Ang University, Seoul, South Korea
[c] Department of Interior Architecture & Built Environment, Yonsei University, Seoul, South Korea

ARTICLE INFO

Article history:
Received 27 October 2015
Received in revised form 5 February 2016
Accepted 16 February 2016
Available online 21 February 2016

Keywords:
Annual daylight simulation method
Daylight illuminance
Sky conditions
Radiance
Daylight coefficient approach
Sun-matching method

ABSTRACT

An annual daylight simulation method (ADSM) has been developed in this study to predict daylight illuminance under diverse sky conditions. The ADSM simulation results were validated by comparing them with Radiance software simulation results and field measurements. Classroom and small private office space facing south and north were used for validation. A classroom facing north and south was used for simulation of ADSM and Raidnace. Field measurements were conducted in a small private office space. Simulation of ADSM was conducted for the conditions of measurements to examine the differences between the results

The results indicated that the daylight illuminance levels computed by ADSM and by Radiance correlated strongly under various sky conditions. Daylight coefficient approach and sun-matching method of ADSM were recommended to achieve higher prediction accuracy. The ADSM simulation results were consistent with actual field measurements of illuminance, even though they varied in accuracy under various sky conditions. The illuminance levels achieved from ADSM and field measurements correlated with each other strongly. Difference ranges between illuminance levels from measurements and simulations were effectively reduced when daylight coefficient approach of ADSM for sky was used with any other computational algorithms of ADSM for the sun.

© 2016 Elsevier B.V. All rights reserved.

1. Introduction

The application scope of energy simulation has been extended from individual buildings to complex objects such as building clusters, communities, and cities to support the management of energy flows within the boundary of a microgrid including electrical and thermal loads, local generation, renewable sources and energy storage [1,2]. Detailed energy simulations of hourly and sub-hourly energy demands for individual buildings enable accurate estimation of energy demands for combinations of buildings, such as communities and cities, allowing decisions to be made regarding the use of local renewable energy for optimum energy consumption [3,4].

Among energy uses in buildings, lighting comprises a large portion of energy consumption. For instance, in office buildings, lighting comprises up to 43% of energy consumption [5]. Hence, lighting energy consumption and savings need to be predicted to determine their effect on heating and cooling loads. One good way to save lighting energy is to utilize daylight, by employing advanced automatic dimming control systems. In case of the control system is employed, the incoming daylight at photosensors and desktops should be predicted accurately.

For this reason, a variety of annual daylight simulations have been used extensively to accurately compute lighting energy consumption and to predict the influence of lighting on heating and cooling loads. Annual daylight simulations have been proposed based on two different methods. One is based on a daylight coefficient approach, which considers luminance from sky surfaces, and the other is based on interpolation between clear and overcast skies based on sky cover, hourly effective sunshine probability, cloud cover, sky clearness, and brightness [6–13].

Representative simulation software packages that use the daylight coefficient approach are DAYSIM, ESP-r, and XDAPS. These all consider hourly or sub-hourly sky luminance distributions over a complete year [11–13]. Software employing interpolation methods include SPOT and ADELINE. These consider a limited number of sky conditions [8,9]

* Corresponding author. Fax: +82 2 313 3139.
E-mail addresses: younju.yoon@samsung.com (Y. Yoon), gilerbert73@cau.ac.kr (J.W. Moon), sooyoung@yonsei.ac.kr (S. Kim).

http://dx.doi.org/10.1016/j.enbuild.2016.02.030
0378-7788/© 2016 Elsevier B.V. All rights reserved.

Nomenclature

ω_{sun}	Solid angle of the sun (sr)
$\omega_{sky\ patch}$	Solid angle of a sky patch (sr)
$E_{ref,sun}$	Reflected illuminance contribution from the sun (lx)
$DC_{ref,sky\ i}$	Reflected component of daylight coefficient from sky patch i (where, i = 1, 2, 3, 4)
L_{sun}	Luminance of the sun (cd/m^2)
$W_{sky,i}$	Weighting factor for sky patch i (where, i = 1,2,3,4)
$W_{sun,i}$	Weighting factor for sun i
$E_{sun,test\ date}$	Illuminance from the sun on a test date (lx)
$E_{rep.sun,i}$	Illuminance from the representative sun i (lx)
$E_{rep.sun,j}$	Illuminance from the representative sun j (lx)
Solar radiance$_i$	Solar radiance for the representative sun i (W/m^2/sr)
Solar radiance$_{test\ date}$	Solar radiance for test date (W/m^2/sr)

Recent studies on the daylight coefficient approach with the Perez sky model have shown that annual daylight simulation at hourly or sub-hourly time steps can be performed using the daylight coefficient method with reasonable computation time and accuracy for clear and overcast skies [6,7,14,15]

DAYSIM is based on a modified version of Radiance and compute illuminance contribution from the sky using the daylight coefficients approach. The solar contribution is calculated using 65 representative latitude-dependent solar positions lying along the sun path on certain days of the year. The illuminance due to the sun for a given time was derived by interpolating the values of the four nearest sun positions to the actual sun positions according to time and altitude differences.

Another tool called Dynamic Daylighting Simulations (DDS) also includes the daylight coefficient approach for annual daylight simulation. However, DDS uses a different scheme for the calculation of the direct and reflected solar contributions to improve accuracy for some cases in which illuminance measurement points are subject to sudden changes in solar exposure [16]. DDS comprises 2305 evenly distributed direct solar positions and 145 indirect solar positions located at the center of each of 145 sky patches.

The approximation of a given sum location to one of 65 and 2,305 pre-calculated sun positions cause errors in predicting the illuminance contribution from direct sunlight penetration. This problem could be avoided by placing the sun at the correct positions at every time and date.

The sky mixing method used in SPOT blends a clear sky daylight factor with an overcast sky daylight factor for a given hour of day and according to sky cover. The interpolation based on sky conditions causes high errors, especially for partly cloudy sky, since considerable differences arise in the luminance distributions of partly cloudy sky that are generated by interpolating between clear and overcast skies.

Accurate representation of the luminance distribution of the actual sky is a key factor affecting the accuracy of a daylight simulation [13]. Among the various sky models used in daylighting simulations, the Perez sky model is commonly applied because it can generate many sky conditions such as clear, intermediate, and overcast sky using the *gendaylit* program in Radiance [17]. The Perez model uses measured direct normal and diffuse horizontal illuminance to generate a sky luminance distribution, but this is unable to capture discontinuous sky luminance distributions in the measured sky.

As a theoretical sky model, the Perez All-Weather Sky model considers predictable features in the sky luminance distribution, such as horizon zenith gradients and circumsolar effect, but could not account for the position, size and pattern of cloud formation at a given point in time since it is non-deterministic features. This problem causes mean bias error (MBE) of 12–28% and root mean square error (RMSE) of 64–88% for internal illuminance, whereas sky models based on measured sky luminance data show MBE of 5–10% and RMSE of 20–70% when the measured internal illuminances were compared with those computed using the *rtrace* program in Radiance [13,18]

To maximize accuracy in daylighting simulation, it is desirable to use measured sky luminance data. However, utilizing sky luminance values based on actual measurements in simulations is not easy and sky luminance data are available only in limited areas. Contrastingly, easily obtainable weather data include global horizontal irradiance and direct horizontal irradiance, which can be measured with inexpensive irradiance sensors and accessed from national or local weather stations.

Since daylighting simulations that use the measured global and direct horizontal irradiance are the most realistic for actual application, it will be helpful to examine their accuracy to understand the discrepancies between the real illuminance and the simulated illuminance that is ultimately used to estimate the electric lighting energy use.

The objective of the present study is to develop an annual daylight simulation method (ADSM) and to examine its accuracy in the prediction of daylight illuminances over a full year using the sky model generated with measured weather data. To evaluate the accuracy of ADSM, its illuminance results were compared with those of Radiance, which is validated computational software and is well known to provide reliable prediction results under various sky conditions [19–21]. The ADSM illuminance results were also compared with measured illuminance data under various sky conditions.

The ADSM developed in this study include representative sun and sky matching methods and the daylight coefficient-based methods. Compared to dynamic daylighting simulations (DDS), the daylight coefficient approach developed in this study uses a different number of direct sun positions. DDS uses 2305 sun positions lying along the annually occurring sun path, whereas the approach used in this study uses actual sun positions that can vary in number depending on the time simulated.

Also, the DDS computes the reflected contributions from 145 sun positions, but the daylight coefficient method developed in this study uses the coefficients of reflected daylight from 145 sky patches to derive the reflected sun illuminances. Comparison between ADSM and existing simulation software is summarized in Table 1.

2. Development of prediction method

In this study, five computational algorithms were developed for sky and sun, and were compared to examine their impact on the accuracy of an annual daylight simulation method (ADSM). The ADSM considers sky and sun separately as light sources. According to the application of light source in computation algorithms, the ADSM is divided into two categories. One category includes a sky matching method and daylight coefficient method for sky. The other category includes a representative sun method and daylight coefficient method for the sun.

2.1. Computational algorithm of ADSM for sun

Two approaches for computation of illuminance due to the sun were developed and compared in this study. One is a sun matching method and the other is a daylight coefficient approach. In the sun matching method, the illuminance contribution from the sun was modeled using 55 representative sun positions, which are the sun

Table 1
Comparison of existing software and annual daylight simulation methods (ADSM).

Illuminance component	Software			
	DAYSIM	Dynamic daylighting simulation (DDS)	ADSM (daylight coefficient approach)	ADSM (sun matching/sky matching)
Direct sun	65 latitude-dependent representative suns for 5 days from sunrise to sunset	2,305 representative suns	Actual suns	55 representative suns for 5 days from 8 a.m. to 5 p.m. (sun matching)
Reflected (indirect) sun		145 representative suns positioned at the centers of 145 sky patches	145 sky patches scaled down to the size of sun	
Direct sky Reflected sky	145 sky patches + 3 ground	145 sky patches	145 sky patches	144 representative skies (sky matching)

positions from 8 a.m. to 6 p.m. for February 21, March 21, April 21, June 21, and December 21. The sun positions on December 21 and June 21, winter and summer solstices, have the lowest and highest altitude angles at given time for a year and those on March 21, equinox, are located in the middle of those two extremes.

These days are frequently used for daylighting simulations as reference days in a year. The sun potions on February 21 and April 21 are almost equally apart from December 21 and March 21 and from March 21 and June 21. If hours outside of this range need to be considered, additional representative suns can be included. The actual sun position is interpolated from the two neighboring sun positions with the same solar time, but from different days with the closest lower and higher solar altitude angles.

The weights assigned to the two representative sun positions are the inverses of their relative linear distances to the actual sun. For example, the two representative positions nearest the sun position at 11 a.m. on May 17 are the 11 a.m. positions on June 21 and April 21. The distances from the actual sun position to these positions are of the ratio 1:1.72, and thus these positions are weighted according to the ratio 0.6333:0.367. Although the sun does not move linearly across the sun angles of each season, but rather more similarly to a sine wave, in this study it was assumed that the sun moved linearly through the equinox and the solstices. This assumption is included in the form of Eq. (1).

$$E_{\text{sun,test date}} = E_{\text{rep.sun},i} \times \frac{\text{Solar radiance}_i}{\text{Solar radiance}_{\text{test date}}} \times W_{\text{sun},i} + E_{\text{rep.sun},j} \times \frac{\text{Solar radiance}_j}{\text{Solar radiance}_{\text{test date}}} \times W_{\text{sun},j} \quad (1)$$

In the daylight coefficient method, the contribution from the sun is divided into direct and reflected components. The direct component of the sun is calculated for all simulation hours using the *rtrace* program in Radiance. Reflected component of the sun, which results from reflection of the global solar illuminance by the surface of the Earth and by any surface intercepting that illuminance, is derived from the reflected component of daylight coefficients from 145 sky patches covering the sky hemisphere and the irradiance values of the suns.

Fig. 1 shows the 145 sky patch that cover the sky hemisphere in order to calculate the contribution of sky patch to calculation point of illuminance in space. The reflected components of daylight coefficients from 145 sky patches are computed by subtracting the direct components from the total (direct + reflected) components of daylight coefficients from 145 sky patches. In this study, single sky patch and four sky patch methods were compared to determine the reflected components of daylight coefficients that were used in the computation of the reflected sun illuminance.

The single sky patch method considers the coefficient of the reflected component of daylight coefficient for the sky patch containing the sun. The method used to derive the illuminance from the reflected daylight coefficient for a single sky patch is explained in Eq. (2). For example, at 11 a.m. on March 21, the sun position is within sky patch 95, as shown in Fig. 2. Therefore, the reflected daylight coefficients from sky patch 95 are used to compute the reflected sun illuminance at this time.

The four sky patch method uses the coefficients of the reflected component of daylight from the four nearest sky patches to the actual sun. Weighting factors based on the inverse distances from the centers of the four sky patches to the center of the sun are applied to these coefficients.

Expressions for the single sky patch and four sky patch methods are given in Eq. (2). For example, the four sky patches surrounding

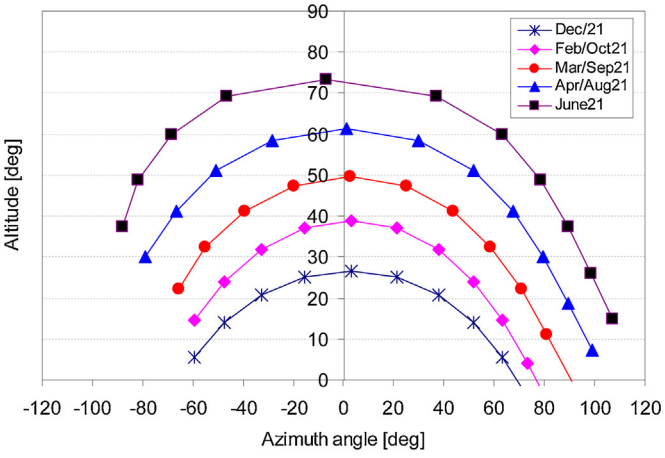

(a) Example of representative sun positions (Site: Boulder, Colorado, USA)

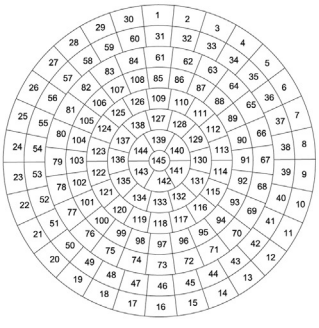

(b) 145 Sky patch

Fig. 1. Representative sun position and sky patch.

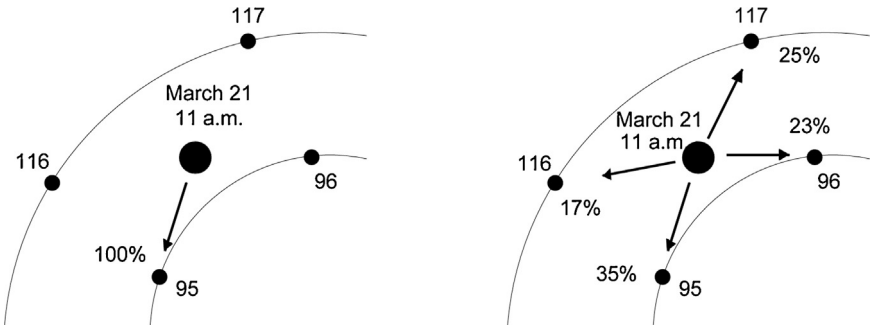

Fig. 2. Explanation for sky patch (left: one sky patch, right: four sky patches).

the sun at 11 a.m. on March 21 are 95, 96, 116, and 117, as shown in Fig. 2. The distances from the center of the sun to the centers of these respective sky patches are of the ratio 0.49:0.73:1.0:0.66. Accordingly, the indirect luminances assigned to these sky patches are 35%, 23%, 17%, and 25%, respectively.

1) Single sky patch condition

$$E_{\mathrm{ref,sun}} = \mathrm{DC}_{\mathrm{ref,sky}} \times L_{\mathrm{sun}} \times \frac{\omega_{\mathrm{sun}}}{\omega_{\mathrm{sky\ \ patch}}}$$

2) Four sky patch condition

$$E_{\mathrm{ref,sun}} = (\mathrm{DC}_{\mathrm{ref,sky1}} \times W_{\mathrm{sky},1} + \mathrm{DC}_{\mathrm{ref,sky2}} \times W_{\mathrm{sky},2} + \mathrm{DC}_{\mathrm{ref,sky3}} \times W_{\mathrm{sky},3} + \mathrm{DC}_{\mathrm{ref,sky4}} \times W_{\mathrm{sky},4}) \times L_{\mathrm{sun}} \times \frac{\omega_{\mathrm{sun}}}{\omega_{\mathrm{sky\ patch}}} \quad (2)$$

To account for the difference in solid angle of a sky patch to a sun, the reflected daylight coefficients of the sky patch are reduced by 724, which is the ratio of solid angle of the sun to solid angle of sky patch. The total illuminance from the sun is calculated by summing the direct solar illuminance and the reflected solar illuminance derived by using the sky daylight coefficients.

Compared to dynamic daylighting simulation (DDS), the daylight coefficient approach developed in this study uses a different number of direct sun positions in the simulation. DDS uses 2305 sun positions lying along the annually occurring sun path, whereas the approach used in this study uses actual sun positions that can vary in number depending on the time simulated. Also, DDS computes the reflected contributions from 145 sun positions, but the daylight coefficient method developed in this study uses the coefficients of reflected daylight from 145 sky patches to derive the reflected sun illuminances. Comparison between ADSM and existing simulation software is summarized in Table 1.

2.2. Computational algorithm of ASDM for sky

In this study, sky matching method and daylight coefficient approach were developed and compared for the computation of sky illuminance. One way to reduce the simulation time for an annual daylight simulation is to reduce the number of simulation cases. The number of simulation cases can be limited by selecting a group of representative sky conditions using an appropriate sky selection criterion.

In the sky matching method, the ratio of vertical illuminance to horizontal illuminance (VH ratio), which was used in the old lumen method for side-lighting to calculate the coefficient of utilization, was used to select representative sky members. Hourly vertical and horizontal illuminances were measured 0.25 m below the top of the window. The VH ratios were computed for every hour of the year, based on the illuminance levels. The VH ratios were grouped according to solar azimuth angles to account for the circumsolar brightening effect, which is not considered in the VH ratios.

The minimum and maximum solar azimuth angles were determined from the hourly solar azimuth angles and the range of solar azimuth angles was divided into several azimuth angle zones. The size of a single azimuth angle zone was computed by dividing the difference between the maximum and the minimum solar azimuth angles by the desired number of azimuth angle zones. Thus, for example, the first azimuth angle zone runs from the minimum solar azimuth angle to an angle that is the sum of that minimum angle and the size of each azimuth angle zone. Then skies were divided into solar azimuth angle zones.

For sky within a specific azimuth angle zone, minimum and maximum VH ratios were determined. Then, representative VH ratios that increased in equal steps from the smallest VH ratio to the largest VH ratio were selected. The increments were determined from the desired number skies per azimuth angle zone. Skies with VH ratios closest to the representative VH ratios were selected as representative skies. This selection of representative skies was repeated for other azimuth angle zones. After a set of representative skies was determined, daylight simulations were performed for only these selected sky conditions.

For each hour, the representative sky having the VH ratio closest to that of the actual sky was used to compute the workplane illuminance distribution for the actual sky, and a scaling factor was applied to account for the difference in the incident exterior vertical glazing illuminance between the actual sky and the representative sky. This scaling factor was the ratio of vertical illuminance of the representative sky to that of the actual sky.

In this study, a sky matching method based on 12 azimuth angle zones and 12 representative skies per azimuth angle zone was used, since this combination was proved to provide the least percent errors and has similar number of skies to the daylight coefficient approach [22]. For example, if the azimuth angle ranged from −89.96° and 107.13° and 12 azimuth angle zones applied, the azimuth angle zone increment would be (107.13° + 89.96°)/12, or 16.42°, and thus the first zone would start at −89.96° and end at −73.53°.

Representative skies whose azimuth angles are assigned to the first azimuth zone and the VH ratios for these skies are computed. If twelve skies per azimuth angle zone were used and the minimum and maximum VH ratios were 0.541 and 0.914, respectively, the VH ratio increment step would be (0.914–0.541)/12, or 0.031. Therefore, the second, third, and fourth representative VH ratios would be 0.572, 0.603, and 0.634, respectively. The first (minimum) VH ratio of 0.541 would be matched to the actual VH ratio of 0.541 and the second VH ratio of 0.572 would be matched to the actual VH ratio of 0.576.

The daylight coefficient approach uses daylight coefficients for 145 sky patches to compute their direct and reflected illuminance contributions, including interreflections at an illuminance measurement point. The daylight coefficient is defined as the ratio of the luminance of each sky patch to the resulting illuminance [23].

Therefore, the total horizontal illuminance produced at the measurement point from a hemispherical sky can be computed by summing the products of the luminances of sky patches and the daylight coefficients for each sky patch. For the annual daylight simulation, a set of daylight coefficients computed for a uniformly luminous sky were multiplied by the luminance values of 145 sky patches for given simulation times. In this study, the *rtcontrib* program in Radiance was used to compute daylight coefficients [18].

3. Validation procedure for prediction method

3.1. Simulation conditions for validation of ADSM against Radiance

In this study, the prediction results of ADSM were compared to those of Radiance to validate the accuracy of ADSM. A typical classroom, located in Boulder, Colorado, USA (latitude: 40°N; longitude: 105.2°W), was modeled to carry out ADSM and Radiance predictions. The layout of this space is illustrated in Fig. 3.

The dimensions of the space were 9.6 m (W) × 9.0 m (D) × 3.3 m (H). A double-pane clear window supported by mullions was installed at the main façade. The dimension of the façade covered by the window was 9.6 m × 2.2 m, and thus the ratio of window area to wall area on the façade was 66.67%. The light transmittance of the window was 67%. The surface reflectances of the ceiling, wall, and floor were assumed to be 70%, 50%, and 25%, respectively, and the reflectance of the outdoor ground was assumed to be 20%, according to general guideline for lighting design [24].

No classroom furniture was placed in the space, and no electric lighting system was operated to allow prediction of daylight illuminance only under various sky conditions. To examine the effect of sun and sky on daylight illuminance, the façade containing the window was assumed to face north and south in separate simulations. No shading device on window and exterior obstructions neighboring the space were considered.

For the modeled space, illuminance sensors facing upward with no tilt angle were assumed to be installed at calculation points shown in Fig. 3. Overall, 21 calculation points were assumed to be installed at the height of 0.75 m, which is generally used as the desktop height in lighting simulations. A single point at the exterior glazing was used for computing exterior vertical and horizontal illuminances. Horizontal illuminance levels at the calculation points under diverse daylight conditions were computed theoretically using ADSM and Radiance.

The TMY2 weather data for Boulder were utilized to simulate Perez luminance distributions for every hour of the year [25–27]. Computer simulations used in this study included clear, intermediate, and overcast sky conditions, which were categorized by the opaque sky cover of the TMY2 weather data. The opaque sky cover represents the amount of sky dome in tenths blocked by clouds or other conditions hindering the observation of sky. According to the classification used, higher numbers correspond to lower chances to observe the sky. The opaque sky covers for a completely clear sky and an overcast sky are 0 and 10, respectively and numbers between 1 and 9 indicate intermediate sky conditions.

Simulations were conducted for the 21st day of March, June, September, and December on an hourly basis from 8 a.m. to 17 p.m. to consider representative sun positions throughout the year. Table 2 summarizes the daylight conditions used for ADSM and Radiance simulations. Table 3 summarizes the opaque sky cover data used for various days and times used in the simulations.

Table 2
Daylight conditions for simulations of ADSM and Radiance.

Orientation	Shading	Day	Time
South	No blind	March/21, June/21	08:00–17:00
North	No blind	September/21, December/21	(hourly base)

The simulations parameters for the *rtrace* program and the *rtcontrib* program are the below. The rtrace program was used for the sky matching method, the sun matching method and the reference Radiance simulations while rtcontrib was used for computing daylight coefficients.

rtrace–ab 7–ad 2048–as 64–ar 32–aa 0.1–lw 0.04

rtcontrib–ab 10–ad 204800–lw 0.0001–as 0–aa 0

For the all prediction results of ADSM and Radiance, statistical analysis using linear regression with analysis of variance (ANOVA) was used in order to investigate the relationship between them. ANOVA is a type of statistical models which is generally used to examine the difference in variation between data groups. It evaluates the importance of factors by examining the response variables at various factor levels, as many reference material indicate [28–30].

ANOVA is effectively used to examine variables for statistical significance. For the ANOVA test, continuous variables should be set and any categorical factor needs to be determined. The statistical significance is determined by a ratio of two variances based on '*F*' test result, primarily.

In addition to the ANOVA test, frequency analysis was conducted for the percent difference in predicted daylight illuminance between ADSM and Radiance to investigate their deviation. Statistical indices such as root mean square error(RMSE) and coefficient of variation of the root mean square error (CV(RMSE)) were used to examine deviations between the illuminance values.,

3.2. Experimental conditions for validation of ADSM against field measurement

As a part of the process of validating ADSM, field measurements were conducted in a full-scale mock-up model space. Measurement results under various sky conditions were compared with ADSM simulation results to examine the accuracy of ADSM. The full-scale mock-up model was constructed on the rooftop of a university building located in Seoul, South Korea (latitude: 37.10°N, longitude: 126.58°E). The layout and view of the model space is shown in Fig. 4. No exterior obstruction was considered for modeling the space. The rooftop of a building was painted with green colored water-proofing paint.

The dimensions of the model space were 3.6 m (W) × 4.2 m (D) × 2.65 m (H). A double-skin envelope system consisting of external envelope, internal envelope and cavity was installed at the main façade. The dimensions of the cavity were 3.6 m (W) × 0.9 m (D) × 2.65 m (H). The long axis of the full-scale mock-up space was tilted 22° toward the east from the north–south axis.

The internal envelope, external envelopes, and side surface of the cavity were covered with the same double-pane glazing as that used in the classroom model. The top of the cavity was covered with acoustic panel board, and no light was allowed to penetrate. The transmittances of the glazing for light and solar irradiance were 62.1% and 34.8%, respectively. Heat transfer coefficient (*U*-value) and solar heat gain coefficient (SHGC) of double-pane glazing were 2.69 W/m^2 K and 0.43, respectively. No shading device was used for the internal or external envelope. The floor of cavity was finished with light beige linoleum.

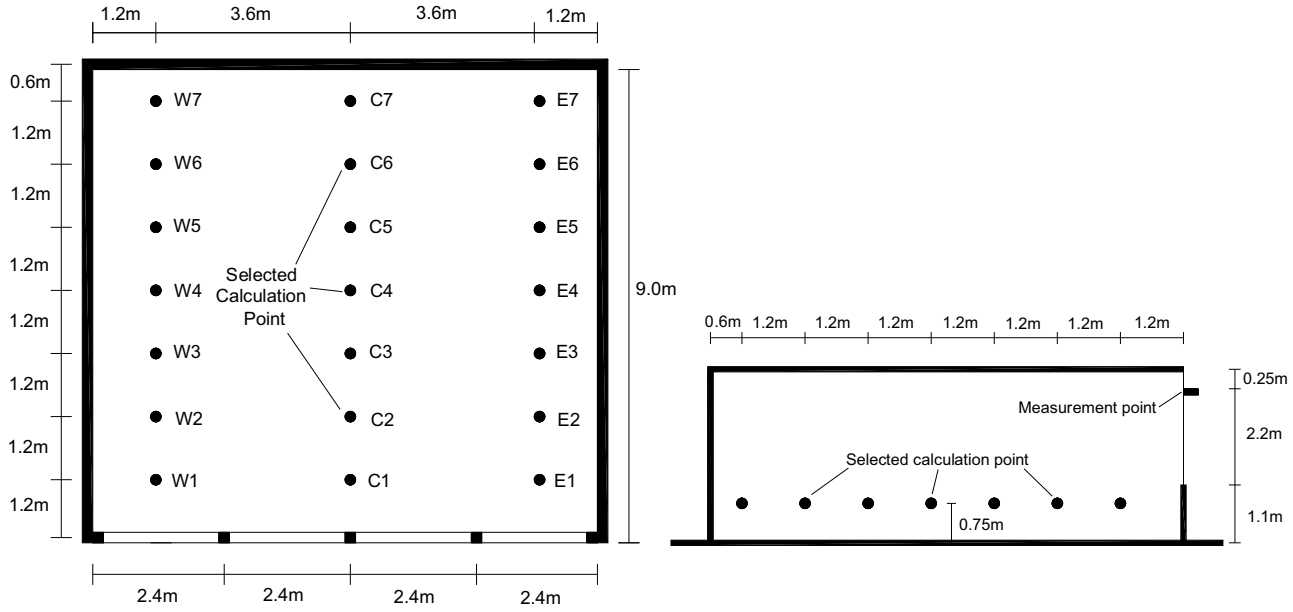

Fig. 3. Layout of space and calculation point (W1–W7, C1–C7, E1–E7).

Table 3
Opaque sky cover for selected day and time according to TMY2 weather data.

Time	08:00	09:00	10:00	11:00	12:00	13:00	14:00	15:00	16:00	17:00
March/21	5	5	4	4	5	7	8	9	9	10
June/21	0	0	0	1	2	2	3	8	5	9
September/21	7	10	10	9	8	9	9	10	10	10
December/21	3	3	2	3	1	1	6	8	7	N/A

The full-scale mock-up model space was furnished like a small office. White wallpaper was used to cover the walls and light beige linoleum was installed on the floor. The wall and floor materials used generated no specular reflection. A suspended grid of 0.6 m × 0.6 m unit cell size was used to hold lighting fixtures. Six recessed-type fluorescent lighting fixtures with T8 lamps and louvers were installed on the ceiling. The area formed by the grid array was covered with white acoustic panel board, except the six positions where lighting fixtures were installed. The lighting fixtures were completely turned off throughout all field measurements in order to examine the effect of daylight on the indoor illuminance of the space.

To collect daylight illuminance at desktop and potential photosensor positions under diverse sky conditions, three photometric sensors were installed on ceiling, desktop and backwall of space. The sensor position is illustrated in Fig. 4. The sensors installed on ceiling and backwall had no shielding conditions and aimed normal to the floor and window, respectively. The sensor positioned on desktop aimed normal to ceiling.

Field measurement data were collected daily from January 2010 to December 2010 to investigate the change of indoor daylight illuminance under diverse actual weather conditions. The monitoring interval for illuminance was one minute and the daylight illuminance levels at the various positions were collected from 07:00 to 18:00. For continuous data monitoring, an automatic data logging system with an accuracy range of 2.5 mV and a photometric sensor with a deviation range of 1% were used [31,32]. This monitoring system and sensor were used in previous studies [33,34].

The conditions of the full-scale mock-up model used in the field measurements were equally modeled by ADSM. The reflectances of ceiling, wall, floor and exterior ground were assumed to be 80%, 60%, 40% and 30%, respectively. The measured global horizontal irradiance and direct normal irradiance were used to generate Perez sky models at hourly intervals. The direct normal irradiance was calculated from the direct horizontal irradiance, and was then divided by the zenith angle of the sun for each given time used in field measurements.

In order to validate the computation accuracy of the ADSM, the prediction results from the ADSM simulation were compared with field measurement data. First, the daylight illuminance monitored in measurements represents the combined influence of sun and sky simultaneously. The predicted illuminance of ADSM represents the effect of sun and sky separately. Thus, combination of ADSM was employed in order to compare measured and predicted illuminance.

Next, linear regression analysis with analysis of variance (ANOVA) was employed to examine the correlation between results of field measurements and ADSM computations. Finally, frequency analysis for the percent differences between measured and predicted results them was performed. Finally, statistical indices such as root mean square error(RMSE) and coefficient of variation of the root mean square error (CV(RMSE)) were used to examine deviations between the illuminance values.

4. Results

4.1. Comparison of ADSM and Radiance simulation results

Prediction results of Radiance and ADSM simulations were examined under the diverse sky conditions based on the TMY2 data to validate the ADSM prediction results. Daylight illuminance levels at the 21 sensor positions shown in Fig. 3 were computed for each given day, time, and opaque sky cover for the sky conditions summarized in Table 3.

(a) View of full-scale mock-up model (left side from vertical center line was used for measurement)

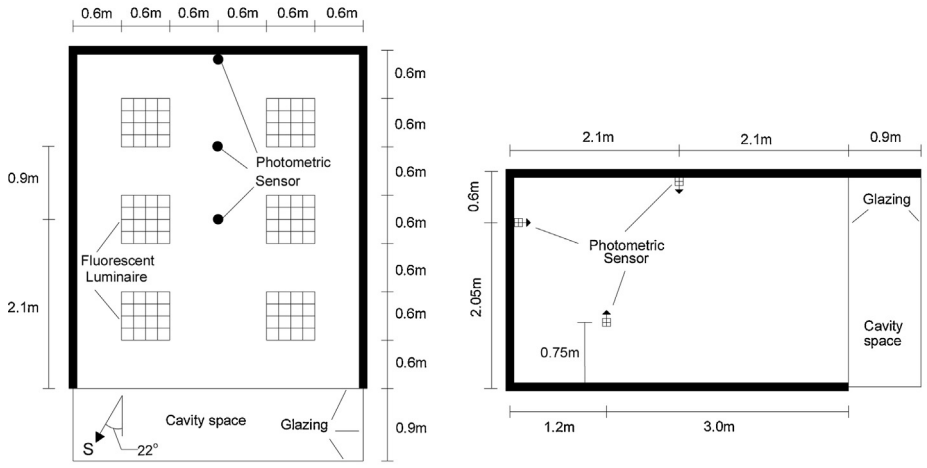

(b) Layout of full-scale mock-up model and photometric sensor position

Fig. 4. Full-scale mock-up model.

Among the ADSM simulation results, some selected examples of illuminance variation for selected calculation points and days are shown in Figs. 5–8 . Overall, the ADSM and Radiance results for daylight illuminance at calculation points showed narrow ranges of difference under the given simulation conditions, except for several cases.

Fig. 5(a) and (b) compares the daylight illuminance at point C6 in March for the south-facing conditions summarized in Table 2. Fig. 6(a) and (b) indicates the difference of daylight illuminance at point C2 in June for the south-facing conditions. For intermediate sky conditions, use of the sky-matching method generated wider ranges of difference compared to the daylight coefficient approach method. For instance, the maximum illuminance difference between Radiance and the sky-matching method was 138 lx during March, when the opaque cover sky was 7. In June, the maximum difference between them was 143.7 lx.

Compared to the sky-matching method, the daylight coefficient approach method generated less deviation from the Radiance result. Over the entire data set used in the simulations, the mean and standard deviation of the difference in illuminance between Radiance and the daylight coefficient approach method were 1.53 lx and 26.62 lx, respectively.

The daylight coefficient approach using one sky patch for the sun generated a wider range of difference under intermediate sky conditions. The maximum differences at point C6 in March and point C2 in June were 160.4 lx and 607.1 lx, respectively. The maximum differences occurred under intermediate sky conditions with opaque sky cover of 4 and 8. The sun-matching and daylight coefficient approach using four sky patches generally produced similar illuminance levels. For the majority of sun and sky predictions, the Radiance and ADSM prediction results deviated narrowly from each other.

Fig. 7(a) and (b) shows the simulation results of ADSM and Radiance at C2 for the north-facing conditions in March and June. Fig. 8(a) and (b) indicates the difference of daylight illuminance at point C4 in September for the north-facing conditions. Similar to the results for the south-facing conditions, ADSM sky predictions varied more from the Radiance results than the prediction of ADSM sun. In the case of ADSM for sky, the use of the sky-matching method generated greater deviation from Radiance in June than the result by the daylight coefficient approach method.

Also, the deviation increased as the opaque sky cover increased. For instance, the deviations for point C2 in June were 37.7 lx and 63.3 lx when the opaque sky cover was 2 and 9, respectively. The deviation in September was also the greatest when the sky-matching method was used. Wide ranges of deviation occurred when the opaque sky cover was higher than 7. For instance, at point C4 the maximum deviation was 271 lx when the opaque sky cover was 10. The daylight coefficient approach method produced narrower deviations over the entire time periods.

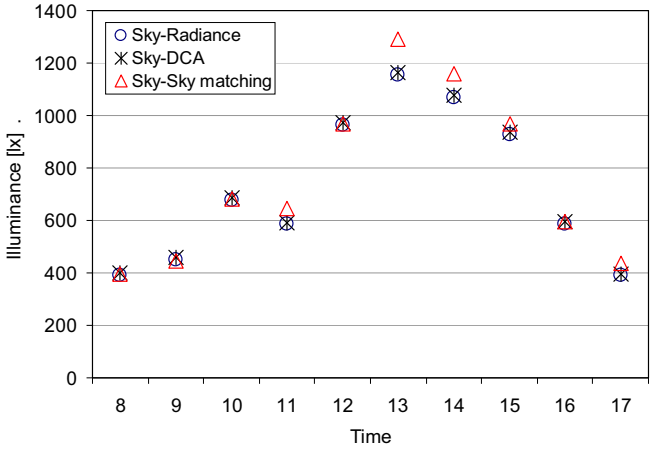

(a) Illuminance from sky on March 21

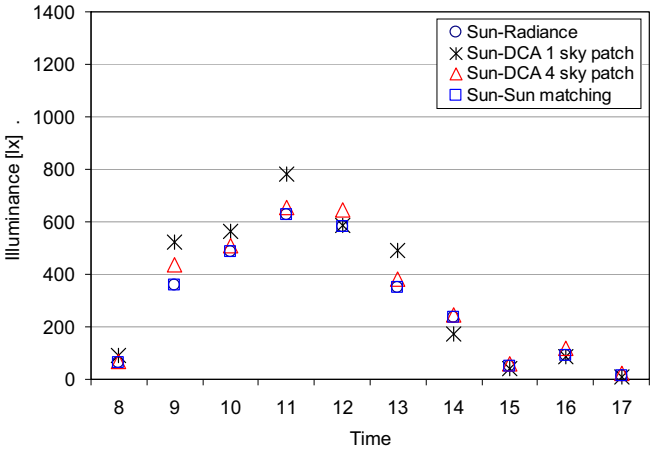

(b) Illuminance from sun on March 21.

Fig. 5. Comparisons of daylight illuminance computed by ADSM and Radiance (south-facing, point C6).

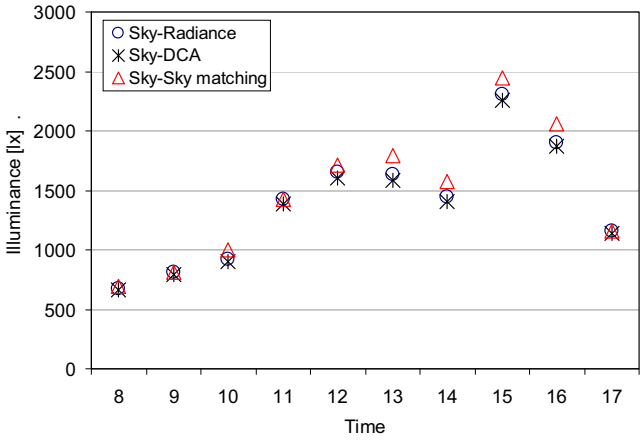

(a) Illuminance from sky on March 21

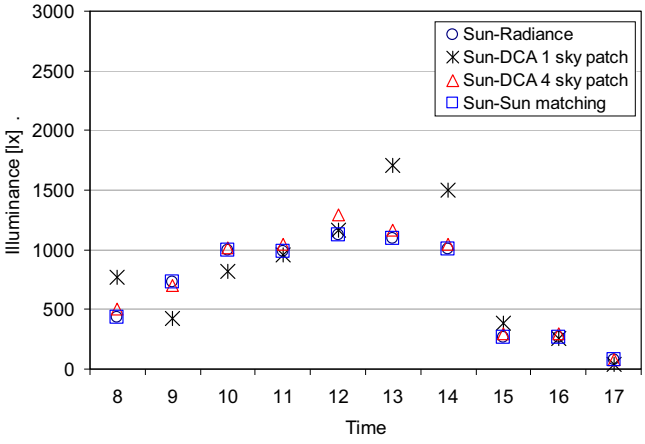

(b) Illuminance from sun on March 21

Fig. 6. Comparisons of daylight illuminance computed by ADSM and Radiance (south-facing, point C2).

The ADSM results for the sun deviated insignificantly from those of Radiance. Compared to the results for south-facing conditions, the deviations by all three computational methods for the sun were reduced over the entire time periods. The maximum deviation at point C4 in September was 75.7 lx, when the opaque sky cover was 8 at noon.

The results imply that using the sky-matching method in ADSM yielded less accurate predictions of daylight illuminance when observation of the sky was hindered by cloud cover intensively. It appears that the accuracy in the prediction of daylight illuminance by ADSM increases when the influence of direct sunlight on indoor space was not available.

4.2. Statistical relationship between ADSM and Radiance simulation results

To examine the relationship between the prediction results of ADSM and Radiance for a given time and day, linear regression analysis with analysis of variance (ANOVA) was employed. For this analysis, the entire simulation results generated by ADSM and Radiance at all calculation points and during entire time periods for all cases listed in Table 2 were used as variables in correlation models.

Table 4 summarizes the coefficients of determination (r^2) for the linear relationships. For each computational method under simulation cases, linear relationship between illuminance by Radiance and ADSM at point C5 for south-facing conditions is shown in Fig. 9(a) and (b). The relationship at point C3 for north-facing is shown in Fig. 10(a) and (b). Table 5 lists ANOVA test results for all regression models. The results indicated that strong linear relationships existed between the ADSM and Radiance simulation results for selected calculation points, such as C5 for south-facing conditions and C3 for north-facing conditions.

Overall, r^2 ranged from 0.638 to 1.0, and the majority of r^2 results were greater than 0.9. The regression models for the selected cases were considered acceptable at the significance level of 0.01. This result implies that the relationship between the ADSM and Radiance simulation results was statistically significant. For ADSM for sky under the cases shown in Table 2, the correlations between the daylight coefficient approach method and Radiance were stronger than those between the sky-matching method and Radiance.

In the case of ADSM for the sun under south-facing conditions, the correlation between the sun-matching method and Radiance was strong. The daylight coefficient approach with four sky patches yielded stronger correlations than the daylight coefficient approach with one sky patch. The correlation with Radiance of the daylight coefficient approach with four sky patches under north-facing conditions was slightly stronger than that of the sun-matching method. This appears to have occurred due to the absence of sun in the northern sky, when north-facing conditions with no blinds were considered in the simulations.

Table 4
Coefficient of determination (r^2) between illuminance from ADSM and Radiance.

Point	Comparison methods for south-facing					Comparison methods for north-facing				
	#1	#2	#3	#4	#5	#1	#2	#3	#4	#5
Outdoor	0.996	1.0	1.0	1.0	1.0	0.920	1.000	0.976	0.996	0.968
C1	0.976	1.0	1.0	1.0	0.939	0.676	0.982	0.964	0.996	0.974
C2	0.960	1.0	0.893	0.994	0.998	0.746	0.986	0.972	0.996	0.974
C3	0.972	1.0	1.0	1.0	1.0	0.808	0.988	0.976	0.994	0.976
C4	0.982	1.0	1.0	1.0	1.0	0.865	0.990	0.974	0.996	0.978
C5	0.984	1.0	0.914	0.994	1.0	0.897	0.992	0.962	0.996	0.980
C6	0.980	1.0	0.906	0.990	1.0	0.903	0.994	0.976	0.996	0.982
C7	0.968	0.998	0.821	0.964	1.0	0.889	0.996	0.958	0.996	0.984
W1	0.970	0.998	1.0	1.0	0.980	0.638	0.982	0.966	0.996	0.974
W2	0.966	1.0	0.998	1.0	1.0	0.704	0.984	0.964	0.996	0.974
W3	0.978	1.0	1.0	1.0	1.0	0.767	0.986	0.968	0.996	0.976
W4	0.984	1.0	1.0	1.0	1.0	0.828	0.988	0.974	0.994	0.978
W5	0.982	0.998	0.994	1.0	1.0	0.878	0.990	0.968	0.996	0.980
W6	0.972	0.998	0.994	1.0	1.0	0.897	0.992	0.972	0.994	0.982
W7	0.945	0.996	0.837	0.865	1.0	0.885	0.994	0.968	0.996	0.984
E1	0.968	0.998	1.0	1.0	0.980	0.663	0.980	0.968	0.994	0.972
E2	0.960	1.0	0.998	1.0	1.0	0.728	0.984	0.974	0.996	0.972
E3	0.980	1.0	0.998	1.0	1.0	0.789	0.986	0.968	0.996	0.976
E4	0.990	1.0	0.998	1.0	1.0	0.845	0.990	0.972	0.996	0.976
E5	0.992	1.0	0.912	0.917	1.0	0.887	0.992	0.970	0.994	0.978
E6	0.986	1.0	0.990	0.994	1.0	0.904	0.994	0.968	0.992	0.980
E7	0.976	0.998	0.806	0.882	1.0	0.897	0.996	0.955	0.992	0.980

#1: Radiance vs. skymatching method of ADSM
#2: Radiance vs. daylight coefficient approach of ADSM.
#3: Radiance vs. daylight coefficient approach with 1 sky patch of ADSM.
#4: Radiance vs. daylight coefficient approach with 4 sky patches of ADSM.
#5: Radiance vs. sunmatching method of ADSM.

Table 5
Linear relationship between illuminance from ADSM and Radiance for selected calculation points.

Case & point	Computation method	Statistics					ANOVA
		Variable	Unstandardized coefficients		t	Sig.	
			B	Std. error			
South-facing, C5	#1	Constant	−10.795	17.519	−0.62	0.54	$F(38,1) = 2370.4$,
		C10	1.016	0.021	48.69	0.00	$r^2 = 0.985$, Sig. = 0.00
	#2	Constant	2.658	2.680	0.99	0.33	$F(38,1) = 96{,}996.3$,
		C10	0.994	0.003	311.44	0.00	$r^2 = 1.0$, Sig. = 0.00
	#3	Constant	64.660	28.240	2.29	0.03	$F(38,1) = 392.03$,
		C10	0.874	0.044	19.80	0.00	$r^2 = 0.914$, Sig. = 0.00
	#4	Constant	10.194	9.115	1.12	0.27	$F(38,1) = 5529.1$,
		C10	1.060	0.014	74.36	0.00	$r^2 = 0.993$, Sig. = 0.00
	#5	Constant	−4.477	2.817	−1.59	0.12	$F(38,1) = 51606.3$,
		C10	1.000	0.004	227.17	0.00	$r^2 = 0.999$, Sig. = 0.00
North-facing, C3	#1	Constant	−88.112	52.271	−1.69	0.10	$F(38,1) = 156.5$,
		C6	1.252	0.100	12.51	0.00	$r^2 = 0.808$, Sig. = 0.00
	#2	Constant	7.940	9.656	0.82	0.42	$F(38,1) = 2875.6$,
		C6	0.991	0.018	53.63	0.00	$r^2 = 0.987$, Sig. = 0.00
	#3	Constant	4.471	4.508	0.99	0.33	$F(38,1) = 1564.2$,
		C6	1.014	0.026	39.55	0.00	$r^2 = 0.977$, Sig. = 0.00
	#4	Constant	−0.174	2.106	−0.08	0.94	$F(38,1) = 7236.3$,
		C6	1.019	0.012	85.07	0.00	$r^2 = 0.995$, Sig. = 0.00
	#5	Constant	5.121	4.485	1.14	0.26	$F(38,1) = 1500.6$,
		C6	0.988	0.025	38.74	0.00	$r^2 = 0.976$, Sig. = 0.00

#1: Radiance vs. sky matching method of ADSM
#2: Radiance vs. daylight coefficient approach of ADSM.
#3: Radiance vs. daylight coefficient approach with 1 sky patch of ADSM.
#4: Radiance vs. daylight coefficient approach with 4 sky patches of ADSM.
#5: Radiance vs. sunmatching method of ADSM.

Frequency analysis was performed of the percent differences in predicted daylight illuminance between ADSM and Radiance to investigate their deviation. Table 6 shows the percent differences of daylight illuminance between ADSM and Radiance for all simulation data considered in this study. Table 7 also summarizes root mean square error (RMSE) and coefficient of variation of the root mean square error (CV(RMSE)) between them. Overall, less deviation occurred when the daylight coefficient approach was used for the sky under all cases considered in this study. Use of the daylight coefficient approach for the sky generated the narrowest range of deviation.

For south-facing conditions, 99.76% of percent differences were within 10% difference range when the daylight coefficient approach for sky was used. This result indicates that the deviation in simulated illuminance between ADSM using the daylight coefficient approach and Radiance can be considered to fall within 10%. In this

Table 6
Percent difference (X) of illuminance from ADSM and Radiance.

Percent difference range (%)	Comparison method for south-facing					Comparison method for north-facing				
	#1	#2	#3	#4	#5	#1	#2	#3	#4	#5
$X < 5$	60.56	91.09	21.00	35.53	83.27	31.50	82.05	25.52	51.40	76.32
$5 < X < 10$	21.00	8.67	13.19	21.98	7.20	15.75	14.16	16.24	27.96	0.25
$10 < X < 15$	11.97	0.24	10.87	17.34	3.66	10.99	1.22	13.31	9.04	2.26
$15 < X < 20$	3.91	0.00	10.74	9.89	1.47	6.72	0.00	9.40	3.66	2.51
$20 < X < 25$	1.95	0.00	10.74	4.40	1.59	8.55	0.85	8.30	1.47	2.13
$25 < X < 30$	0.61	0.00	6.84	4.03	1.59	11.97	1.10	7.69	0.73	5.76
$X > 30$	0.00	0.00	26.62	6.84	1.22	14.53	0.61	19.54	5.74	10.78
Total	100	100	100	100	100	100	100	100	100	100

#1: Radiance–sky matching method of ADSM
#2: Radiance–daylight coefficient approach of ADSM.
#3: Radiance–daylight coefficient approach with 1 sky patch of ADSM.
#4: Radiance–daylight coefficient approach with 4 sky patches of ADSM.
#5: Radiance–sunmatching method of ADSM.

Table 7
Root mean square error (RMSE) between illuminance from ADSM and Radiance.

Orientation	Statistics	Comparison method				
		#1	#2	#3	#4	#5
South-facing	RMSE (lx)	157.97	34.67	164.05	116.71	18.26
	CV (RMSE) (%)	13.21	2.90	22.71	16.15	2.53
North-facing	RMSE (lx)	175.76	46.35	30.43	12.79	22.39
	CV (RMSE) (%)	25.51	6.73	17.90	7.52	13.17

#1: Radiance–sky matching method of ADSM
#2: Radiance–daylight coefficient approach of ADSM.
#3: Radiance–daylight coefficient approach with 1 sky patch of ADSM.
#4: Radiance–daylight coefficient approach with 4 sky patches of ADSM.
#5: Radiance–sunmatching method of ADSM.

case, the RMSE and CV(RMSE) between the predicted illuminance levels was 34.67 lx and 2.90%, respectively. When the sky-matching method was used, 81.56% of the percent differences between ADSM and Radiance were within 10% of percent difference range. In this case, the RMSE and CV(RMSE) were 157.97 lx and 13.21%, respectively.

When the sun-matching method for the sun was used for south-facing conditions, 90.47% of percent differences were 10% of difference range. Also, the RMSE and CV(RMSE) were 18.26 lx and 2.53%, respectively. The percent difference range and CV(RMSE) generated by daylight coefficient approach with one or four sky patches were wider compared to the range of sun-matching method. This implies that daylight coefficient approach using either the one or four sky patch rarely achieved such a narrow range of deviations.

For north-facing conditions, the percent differences varied more widely than those for south-facing conditions. Also 96.11% and 76.57% of percent differences fell into 10% of the difference range when the daylight coefficient approach method was used for the sky and sun-matching method for the sun. For those cases, the CV(RMSE) were 6.73% and 13.17%, respectively. This result implies that the daylight coefficient approach for the sky and sun-matching method for the sun generated closer results than that of Radiance. Like the case for south-facing conditions, use of the daylight coefficient approach for sky with one sky patch generated a wider range of deviations, compared to the rest of method.

In summary, the ranges of deviation between ADSM and Radiance daylight illuminance predictions were most narrow when the daylight coefficient approach method was used for sky and the sun-matching method was used for sun. Thus, using these two methods with ADSM produced the simulation results closest to those of Radiance. The sky-matching method for the sky and daylight coefficient approach with one sky patch for the sun generated wider deviation ranges compared to the rest of methods.

The daylight illuminance levels simulated by ADSM were not fully consistent with those simulated by Radiance under given sky conditions from TMY2 data. However, the ADSM still provided reliable results for the prediction of indoor daylight illuminance. In terms of computation time, the daylight coefficient approach for sky and sun consumes less computation times than the sky matching and the sun matching method since these two matching methods requires the simulation rums same as the number of representative suns and sky positions while the daylight coefficient approach computes annual daylight illuminance in a single simulation run.

4.3. Variation of outdoor illuminance

Field measurements were conducted for the full-scale mock up model space in order to examine the changes of illuminance due to variation in sky conditions throughout the entire data monitoring period. Among the data collected throughout the entire monitoring period, data that show three representative sky conditions, such as clear, partly cloudy, and overcast sky were selected to investigate the influence of sky conditions on indoor daylight illuminance. The variations of global and diffuse illuminance for these three sky conditions are shown in Fig. 11.

As shown in Fig. 11(a), the global and diffuse illuminances under clear sky conditions varied stable patterns. The global illuminance showed noticeable differences between June and December, when solar altitudes were at their extremes for the year. For instance, the maximum global illuminance was 100,100 lx in June and 50,870 lx in December. The diffuse illuminance, which represents illuminance from sky surfaces, also showed stable variations. Unlike the case for global illuminance, the diffuse illuminance in June and December varied within a narrow range. Diffuse illuminance was lower in December than in June, and its maximum values in June and December were 15,340 lx and 9890 lx, respectively.

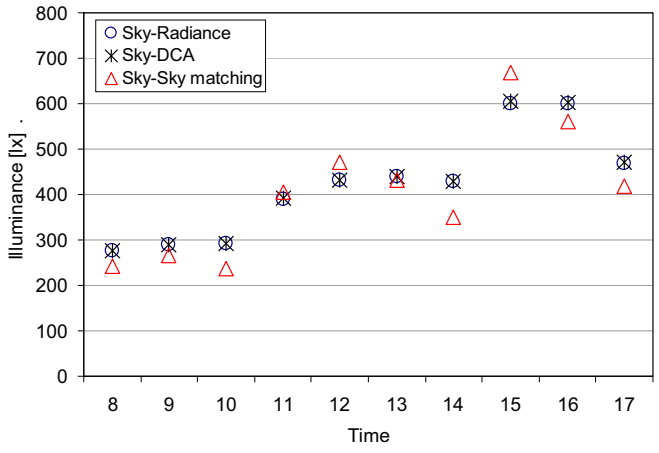

(a) Illuminance from sky on June 21

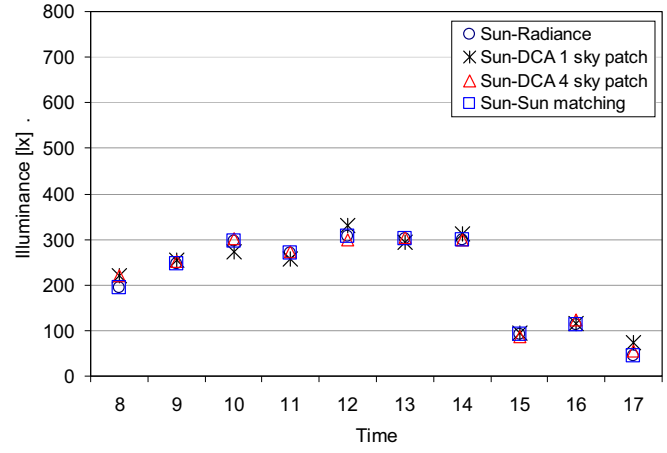

(b) Illuminance from sun on March 21

Fig. 7. Comparisons of daylight illuminance computed by ADSM and Radiance (north-facing, point C2).

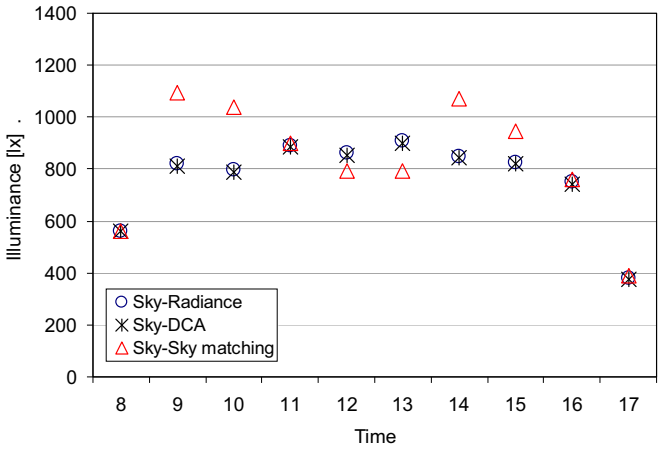

(a) Illuminance from sky on September 21

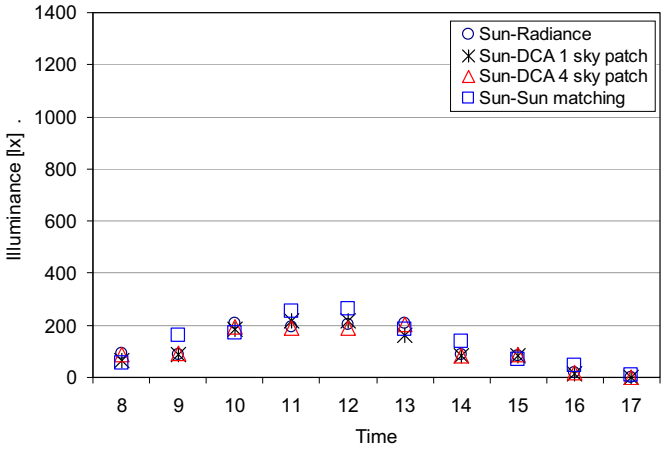

(b) Illuminance from sky on September 21

Fig. 8. Comparisons of daylight illuminance computed by ADSM and Radiance (north-facing, point C4).

Fig. 11(b) shows global and diffuse illuminances for partly cloudy sky in June and December. Unlike the clear sky case, both illuminances varied unstably throughout the monitoring period, except for several hours in December. Illuminance fluctuated frequently among the measured time intervals. The global and diffuse illuminance levels in June were greater than those in December due to the higher solar altitude. The maximum global illuminance was 91,000 lx in June and 42,650 lx in December. The diffuse illuminance also fluctuated unstably. The diffuse illuminance in June and December under partly cloudy sky clearly differed from that in the case of clear sky. The maximum diffuse illuminance was 42,650 lx in June and 21,290 lx in December.

Fig. 11(c) shows the variation of global and diffuse illuminances for overcast sky conditions. Global illuminance remained stable for the majority of measurement periods, except in some morning periods in June. Global illuminance in overcast conditions was slightly greater in June than in December, but the differences were insignificant compared to those of the other two sky conditions. The maximum global illuminance in December was 26,980 lx. Diffuse illuminance also varied stably showing insignificant fluctuation. The illuminance in overcast conditions in June and December were similar except for several cases in the morning, which shows insignificant difference overall. For instance, the maximum diffuse illuminance in December was 23,250 lx.

4.4. Validation of ADSM against field measurement results

Daylight illuminance was measured at three points in the mock-up space shown in Fig. 4. These measurement data were analyzed to investigate the difference between them and the ADSM prediction results. In order to compare the illuminance levels, the illuminance by ADSM was computed according to the combination of computation algorithms for sky and sun, since the daylight illuminance monitored in measurements represent the combined influence of sun and sky simultaneously.

As discussed in Section 2, two algorithms such as daylight coefficient approach (DCA) and sky-matching method were used to compute illuminance by sky. Three algorithms such as the DCA with one sky patch (DCA-1), the DCA with four sky patches (DCA-4), and the sun-matching method, were used to compute sun illuminance. Thus, there were 6 possible combinations of algorithms that could be used to compute sun and sky illuminance, as listed in Table 8.

The comparison between illuminance from field measurements and the variations in illuminance at the three measurement points resulting from the use of each of the six algorithm combinations under selected day and sky conditions are shown in Figs. 12–14 . Overall, illuminance levels predicted by ADSM were consistent with field measurements, although the difference between ADSM

Table 8
ADSM algorithms for combination of sun and sky.

Algorithm	Computation algorithm for sky	Computation algorithm for sun
I	Daylight coefficient approach (DCA)	Daylight coefficient approach with 1 sky patch (DCA-1 patch)
II	Daylight coefficient approach (DCA)	Daylight coefficient approach with 4 sky patch (DCA-4 patch)
III	Daylight coefficient approach (DCA)	Sunmatching
IV	Sky matching	Daylight coefficient approach with 1 sky patch (DCA-1 patch)
V	Sky matching	Daylight coefficient approach with 4 sky patch (DCA-4 patch)
VI	Sky matching	Sun matching

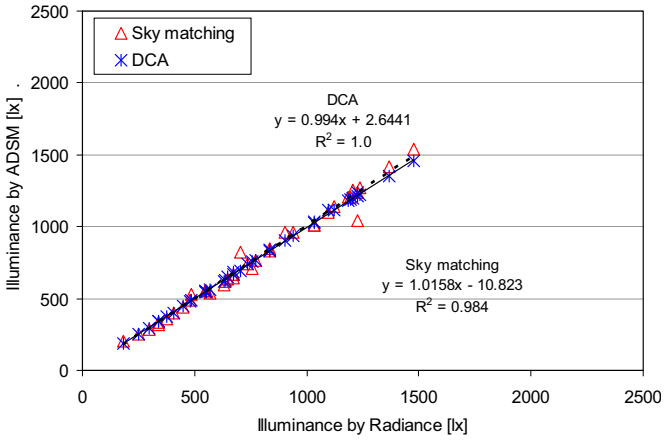

(a) Illuminance from sky

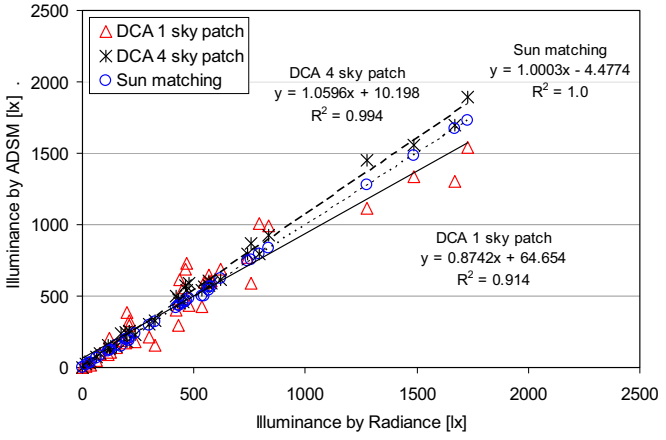

(b) Illuminance from sun

Fig. 9. Correlation between illuminances computed by ADSM and Radiance (south-facing, point C5).

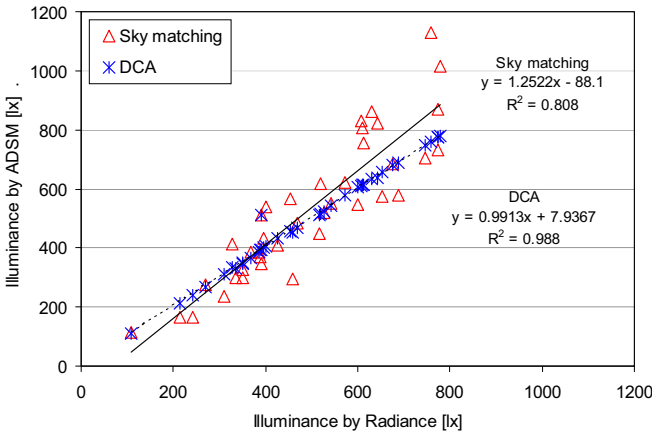

(a) Illuminance from sky

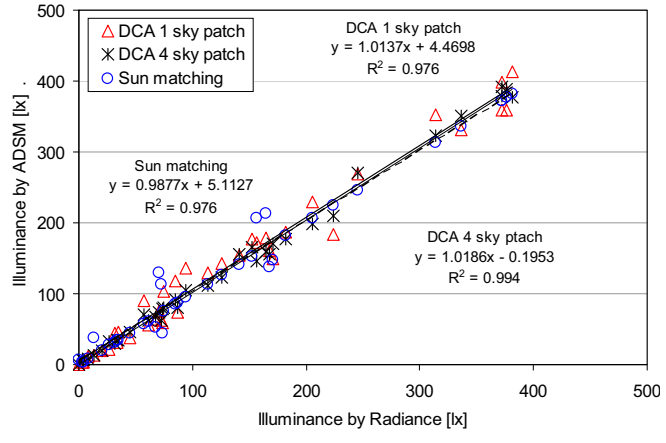

(b) Illuminance from sun

Fig. 10. Correlation between illuminances computed by ADSM and Radiance (north-facing, point C3).

results and field measurements varied among the combinations of algorithms used for the sun and sky.

Fig. 12 shows the illuminance variation on ceiling for a selected day in December under clear sky conditions. Like the measurement results, the prediction results varied stably throughout the day. Overall, the illuminance levels predicted by ADSM were lower than the measured results, and this difference varied among the combinations of algorithms used for the sun and sky contributions.

Among the six algorithm combinations shown in Table 8, algorithm III (DCA for sky and sun-matching method for sun) and algorithm VI (sky-matching for sky and sun-matching method for sun) generated the illuminance levels most similar to the measured values. The rest of the four algorithms generated noticeable deviations from the measurement results. It appears that the sun-matching method is most accurate for modeling the sun contribution, and can be used in combination with either of two sky algorithms to best predict daylight illuminance under daylight conditions. Under clear sky conditions, the illuminance component due to the sun is likely to dominate that of the sky. Therefore, annual simulation methods including the sun matching method, which considers the circumsolar brightening effect, perform better than those using DCA, regardless of the simulation methods used for the sky.

Fig. 13 shows variations in daylight illuminance on backwall under partly cloudy sky conditions in December. The sky was partly cloudy before noon, but clear in the afternoon. The patterns of difference between measured and predicted illuminance were similar to those under clear sky conditions. Overall, the measurement results were greater than the prediction results. Three computation algorithms for sky generated less deviation from measurement results when they were combined with the sun-matching meth-

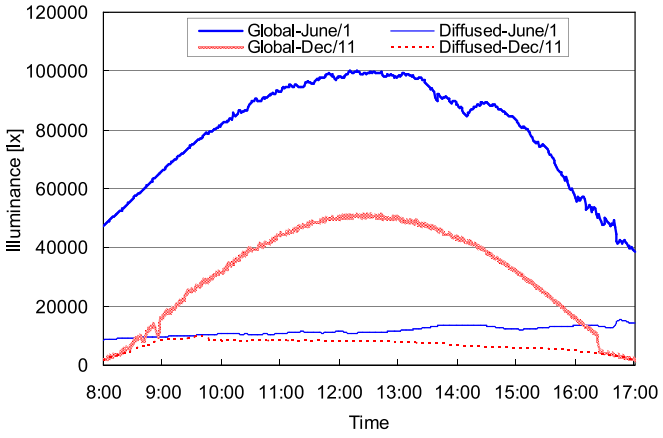

(a) Clear sky

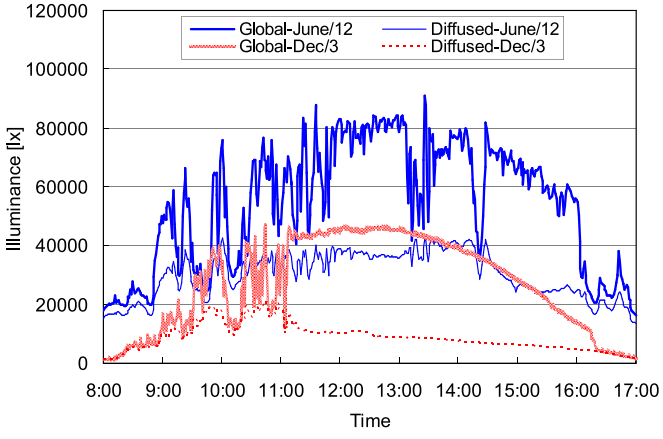

(b) Partly cloudy sky

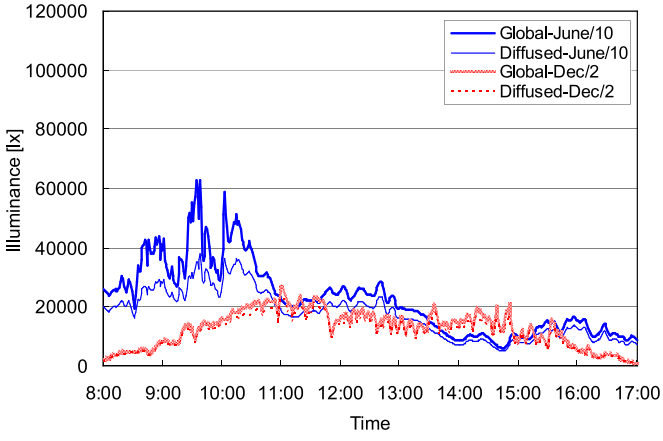

(c) Overcast sky

Fig. 11. Variation of outdoor global and diffused illuminance.

ods for the sun. Daylight coefficient approach with one or four sky patches for the sun produced wider ranges of differences compared with the sun-matching method.

Similar to the results for clear sky conditions, the illuminance differences between measured results and the annual daylight simulation algorithms I, II, IV, and V were greater during hours with less cloud cover compared to those of algorithms III and VI. Therefore,

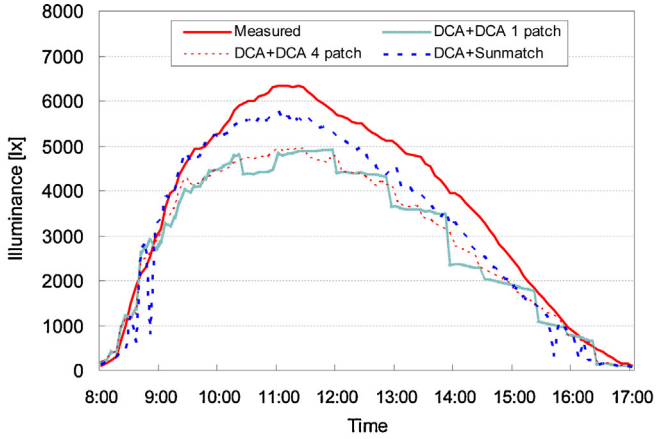

(a) ADSM for sky: Daylight coefficient approach, ADSM for sun: Three methods

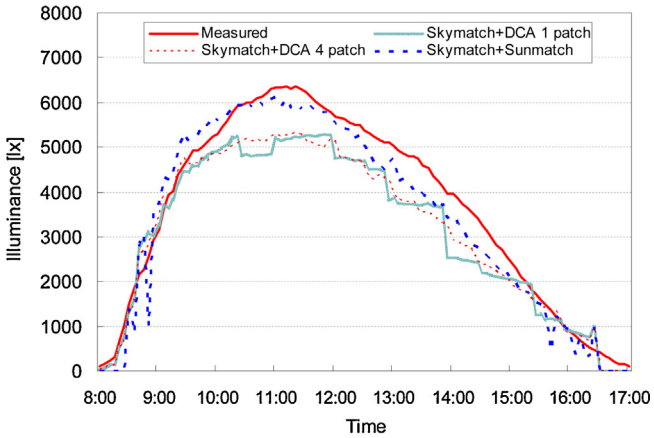

(b) ADSM for sky: Sky matching method, ADSM for sun: : Three methods

Fig. 12. Comparison of measured illuminance and computed illuminances using ADSM for a point at ceiling (clear sky, December/11).

algorithms including the sun matching method performed better than the other algorithms.

Fig. 14 shows variations in daylight illuminance on desktop under overcast sky conditions, in which diffuse illuminance was stronger than direct illuminance. The differences between modeled and measured results were greater than those for clear and partly cloudy sky conditions when the sky-matching method for sky was used with any of the algorithms for sun. Compared with the sky-matching method, use of DCA for the sky yielded less deviation from measurement results when combined with any of the three algorithms for sun. Also, the deviation was least when the illuminances were the lowest.

The illuminance of overcast sky is dominated by the sky contribution due to the minimized impact of the sun. Thus, accurate representation of the luminous distribution of the sky is important in overcast conditions. The sky luminance distribution used for the daylight coefficient method is same as that of the actual sky, whereas the sky matching method estimates the illuminance based on representative skies. Therefore, the daylight coefficient approach is more accurate than the sky matching method for the computation of illuminance under overcast sky conditions.

In this study, linear regression analysis was employed to examine the correlation between results of field measurements and ADSM computations. Coefficients of determination between measured and simulated illuminance levels were examined and

Table 9
Linear relationship between measured and simulated illuminance.

ADSM algorithm	Ceiling		Desktop		Northwall	
	r^2	ANOVA	r^2	ANOVA	r^2	ANOVA
I	0.934	$F(611,1) = 8690.2$ Sig. = 0.00	0.692	$F(623,1) = 1399.9$ Sig. = 0.00	0.907	$F(623,1) = 6070.6$ Sig. = 0.00
II	0.942	$F(611,1) = 9870.6$ Sig.=0.00	0.697	$F(623,1) = 1431.5$ Sig. = 0.00	0.915	$F(623,1) = 6678.7$ Sig. = 0.00
III	0.937	$F(611,1) = 9097.1$ Sig. = 0.00	0.639	$F(623,1) = 1103.6$ Sig. = 0.00	0.922	$F(623,1) = 7416.9$ Sig. = 0.00
IV	0.833	$F(611,1) = 3054.9$ Sig. = 0.00	0.681	$F(623,1) = 1330.8$ Sig. = 0.00	0.797	$F(623,1) = 2452.3$ Sig. = 0.00
V	0.84	$F(611,1) = 3203.3$ Sig. = 0.00	0.686	$F(623,1) = 1360.5$ Sig. = 0.00	0.804	$F(623,1) = 2562.6$ Sig. = 0.00
VI	0.859	$F(611,1) = 3734.9$ Sig. = 0.00	0.631	$F(623,1) = 1062.7$ Sig. = 0.00	0.835	$F(623,1) = 3168.8$ Sig. = 0.00

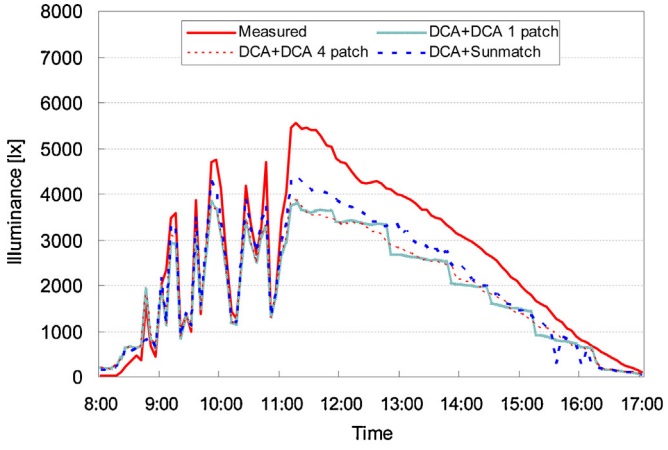

(a) ADSM for sky: Daylight coefficient approach, ADSM for sun: Three methods

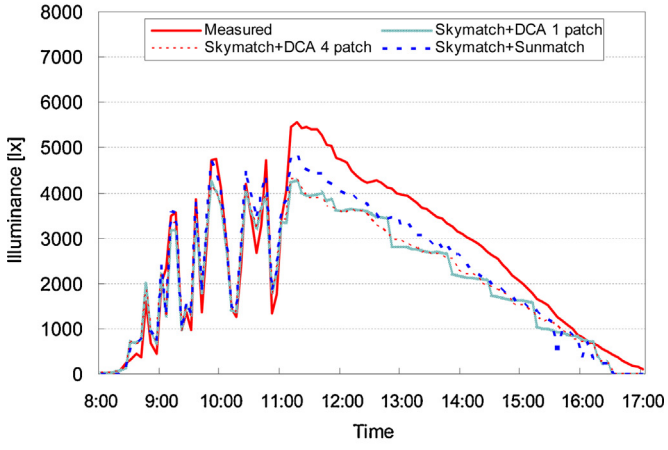

(b) ADSM for sky: Sky matching method, ADSM for sun: : Three methods

Fig. 13. Comparison of measured illuminance and computed illuminances using ADSM for a point at north wall (partly cloudy sky, December/3).

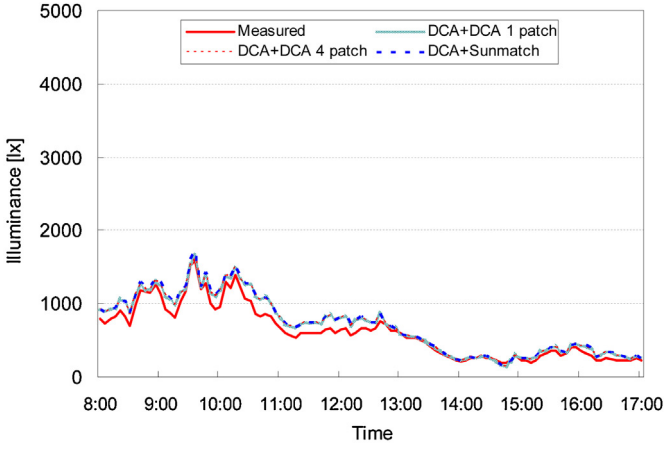

(a) ADSM for sky: Daylight coefficient approach, ADSM for sun: Three methods

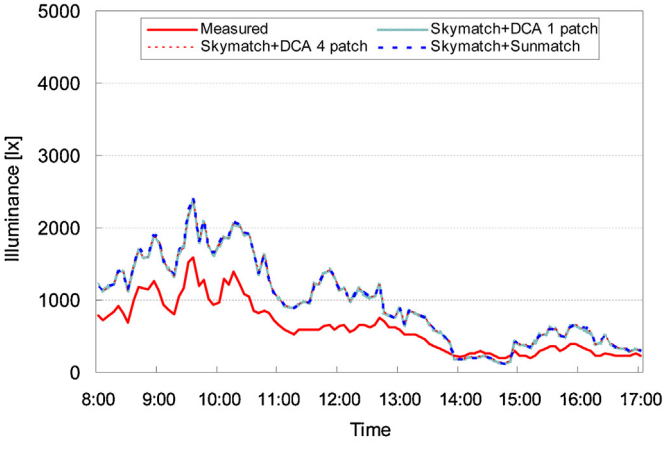

(b) ADSM for sky: Sky matching method, ADSM for sun: : Three methods

Fig. 14. Comparison of measured illuminance and computed illuminances using ADSM for a point at desktop (overcast sky, June/10).

statistical analysis of variance (ANOVA) was used to test the correlation with a significance level. For the relationship, entire results of field measurements were used as the independent variables and ADSM results were used as the dependent variables. The linear relationship and statistical ANOVA test results are summarized in Table 9. Example of scatter plots showing relationship between the variables at three points is shown in Fig. 15.

Overall, the linear regression models were acceptable at the significance level of 0.01. This result implies that the correlation between results of field measurements and ADSM computations was statistically significant. Strong linear correlations existed between measured and simulated results under various sky conditions, since r^2 ranged from 0.631 to 0.942 for all cases. The correlations were relatively stronger when DCA was used in the ADSM to model the sky, compared with those when the sky-matching method was used. The correlation analysis results indicate that the ADSM simulation results strongly correlated with field measurements.

Table 10
Percent difference of illuminance (X) between ADSM and field measurements.

Sensor position	ADSM algorithm	Percent difference range (%)							
		$X<5$	$5<X<10$	$10<X<15$	$15<X<20$	$20<X<25$	$25<X<30$	$X>30$	Total
Ceiling	I	46.98	33.61	11.09	3.92	2.94	0.65	0.82	100
	II	42.09	42.41	7.01	4.08	2.94	0.65	0.82	100
	III	48.94	33.44	7.50	4.40	3.26	1.47	0.98	100
	IV	19.25	26.59	25.45	16.64	5.38	2.61	4.08	100
	V	20.39	26.26	24.80	16.31	5.55	2.61	4.08	100
	VI	22.68	15.82	28.87	18.27	5.22	2.45	6.69	100
Desktop	I	50.24	24.96	12.96	4.00	3.68	2.88	1.28	100
	II	50.56	27.52	10.56	5.28	3.84	2.56	1.28	102
	III	46.40	35.20	5.44	3.36	4.96	4.00	0.64	100
	IV	18.24	39.20	25.92	6.08	2.72	3.68	4.16	100
	V	17.76	42.56	22.56	6.40	2.72	3.68	4.32	100
	VI	16.32	42.08	21.92	6.40	3.36	3.36	6.56	100
North wall	I	41.12	39.20	10.56	4.00	3.04	0.96	1.12	100
	II	40.32	43.36	7.36	3.84	3.04	1.12	0.96	93
	III	46.40	35.84	7.04	3.84	4.48	1.44	0.96	100
	IV	14.24	37.60	28.48	8.48	3.68	2.24	5.28	100
	V	15.20	37.44	26.88	9.28	3.20	2.72	5.28	100
	VI	23.20	19.68	33.60	9.92	3.84	1.92	7.84	100

Table 11
Root mean square error (RMSE) between measured and predicted illuminance by ADSM.

Statistics	Sensor position	ADSM algorithm					
		I	II	III	IV	V	VI
RMSE (lx)	Ceiling	614.66	596.02	478.74	793.07	783.82	776.07
	Desktop	623.36	601.89	532.66	665.29	649.93	612.00
	North wall	648.15	634.92	500.89	715.22	704.23	648.06
CV (RMSE) (%)	Ceiling	32.56	31.57	25.36	42.01	41.52	41.11
	Desktop	39.40	38.04	33.67	42.05	41.08	38.68
	North wall	37.52	36.76	29.00	41.40	40.77	37.52

As a final step to validate the prediction results of ADSM, frequency analysis was conducted. To determine the deviation of simulated illuminances from measured illuminances, the percent differences between them were computed. Table 10 shows the analysis results. Also, Table 11 summarizes root mean square error (RMSE) and coefficient of variation of the root mean square error (CV(RMSE)) between them. The CV(RMSE) for the six algorithm ranged from 25.36% to 42.05%.

For all points considered in this study, algorithms I, II, and III, which employ DCA for sky, showed narrower ranges of difference compared to algorithms IV, V, and VI, which used the sky-matching method for sky. Also, the RMSE and CV(RMSE) for the six algorithms showed similar trends to analysis result of the percent difference.

The algorithm III, which contains daylight coefficient approach for the sky and sun-matching method for the sun, generated the narrowest deviation range compared to the rest of combination of algorithms. For instance, 82.3% of differences were within 10% when algorithm III was used for the sensor positioned at ceiling. This means that the majority of deviations between the simulated and measured illuminances fell within 10%. The CV(RMSE) were and 25.36%. This implies that the prediction can be performed best when daylight coefficient approach for the sky and sun-matching method for the sun were employed in the simulation of ADSM.

Contrastingly, only 37.5% of differences fell within 10% when algorithm VI was used for the sensor at ceiling. In this case, the RMSE and CV(RMSE) were 793.07 lx and 42.01%, respectively This result implies that the combination of sky matching method for the sky and daylight coefficient approach with one sky patch provided less reliable prediction results.

In summary, the deviation range between measured and simulated illuminance can be effectively reduced by using algorithm I, II, or III, which use DCA for sky. This implies that ADSM simulation results are consistent with measurement results. The simulated results were not perfectly consistent with field measurements, but provide statistically reliable results.

5. Conclusions

This study was performed to develop ADSM to predict daylight illuminance under diverse sky conditions. The ADSM simulation results were validated by comparing them with Radiance software simulation results and field measurements. The summary of findings is as follows:

1. The daylight illuminances computed by ADSM and Radiance under various sky conditions based on TMY2 weather data correlated strongly with each other. ADSM results varied least from Radiance results when the daylight coefficient method was used to model sky illuminance and the sun-matching method was used to model sun illuminance. This implies that using the daylight coefficient approach for sky and the sun-matching method for sun in ADSM achieves the highest prediction accuracy.
2. The ADSM simulation results were consistent with actual illuminance levels measured in the field, although the consistency varied under various sky conditions. ADSM underpredicted illuminance levels under clear and partly cloudy sky conditions with lower cloud covers, in which the effect of diffuse daylight illuminance is weak. However, the simulation results were greater under overcast sky conditions, in which the influence of diffuse sky illuminance was strong.
3. Linear regression and ANOVA tests implied that the illuminance levels predicted by ADSM strongly correlated with field measurements, and showed statistical significance with a significance level of 0.01. In particular, when the daylight coefficient

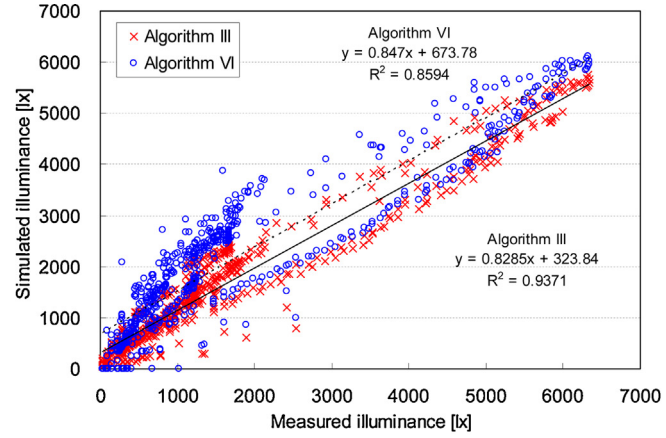

(a) Ceiling

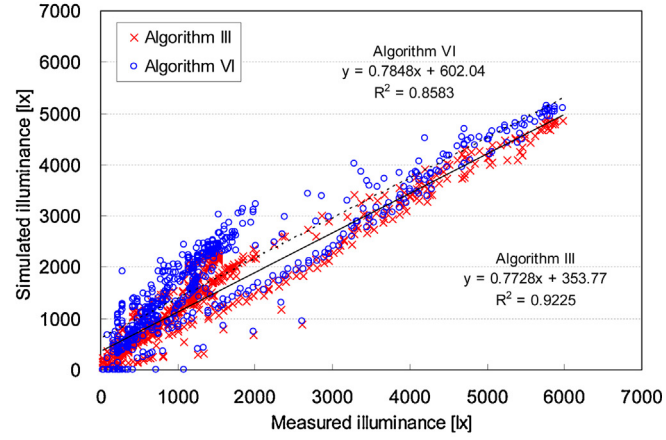

(b) North wall

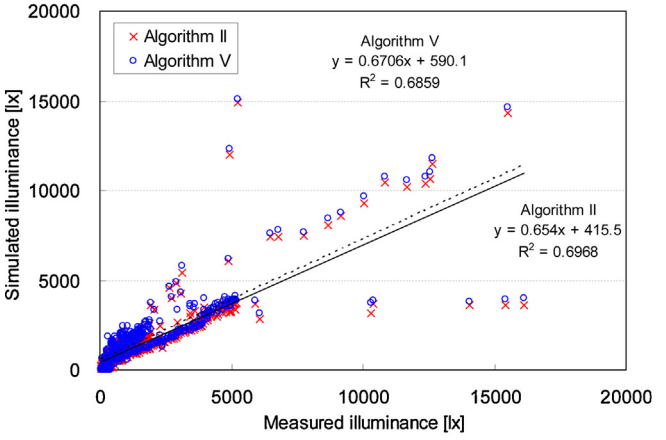

(c) Desktop

Fig. 15. Linear relationship between measured and simulated illuminance.

approach was used to model sky illuminance in ADSM, instead of the sky-matching method, this yielded stronger correlations to field data. All regression models relating ADSM simulation results and measurements were found to be effective at the significance level of 0.01.

4. Differences between measured and simulated illuminance were minimized overall when the daylight coefficient approach was used for sky, in combination with any of the computational algorithms used for the sun. When these methods were used, the majority of percent differences between simulated and measured illuminance were within 10%, under all sky conditions. Among the ADSM variants developed in this study, combining the daylight coefficient approach for the sky and the sun matching method performed best. However, the daylight coefficient approach with 4 sky patches also provides comparable accuracy. Considering the overall computation time, the daylight coefficient approach for the sky and the daylight coefficient approach with 4 sky patches for the sun are the best performer.
5. In this study, the illuminance levels simulated by ADSM were compared with illuminance levels from a well-known simulation software package and with field measurements for some selected conditions. Due to research limitations in research budget and administration supports, field measurements were carried out at a different site than that used in the simulations. Different sites may influence the test results in this study, but the ADSM method developed in this study was considered effective since the daylight illuminance in indoor space are affected by the sun position and amount of clouds in sky.
6. In future studies, equivalent site conditions would be necessary for simulations and measurements. To investigate the differences in illuminance between predictions and measurements, further examinations under various other conditions would also be helpful.

Acknowledgment

This research was supported by the Basic Science Research Program through the National Research Foundation of Korea (NRF) funded by the Ministry of Science, ICT and Future Planning (NRF-2014R1A2A1A11051162).

References

[1] J. Keirstead, M. Jennings, A. Sivakuma, A review of urban energy system models: approaches, challenges and opportunities, Renew. Sustain. Energy Rev. 16 (2012) 3847–3866.
[2] M. Manfren, P. Caputo, G. Costa, Paradigm shift in urban energy systems through distributed generation: methods and models, Appl. Energy 88 (2011) 1032–1048.
[3] K. Janak, I. Macdonald, Current state-of-the-art of integrated thermal and lighting simulation and future issues, in: Proceedings of the 6th International Building-Performance Simulation's Association (IBPSA) Conference (BS'99), Kyoto, Japan, September, 1999, pp. 1173–1180.
[4] R. Guglielmetti, S. Pless, P. Torcellini, On the use of integrated daylighting and energy simulations to drive the design of a large net-zero energy office building, in: Proceedings of the Fourth National Conference of IBPSA-USA: SimBuild 2010, New York, 2010, pp. 301–309.
[5] L. Perex-Lombard, J. Ortiz, C. Pout, A review on buildings energy consumption information, Energy Build. 40 (2008) 394–398.
[6] J. Mardaljevic, Simulation of annual daylight profiles for internal illuminance, Light. Res. Technol. 32 (2000) 111–118.
[7] C. Reinhart, O. Walkenhorst, Validation of dynamic RADIANCE-based daylight simulations for a test office with external blinds, Energy Build. 33 (2001) 683–697.
[8] C. Clevenger, Z. Rogers, Project 6.2 program technology and product design tools, in: SPOT Development Report, Architectural Energy Corporation, Boulder, CO, USA, 2004.
[9] M. Szeman, J. Stoffel, ADELINE 2.0, Radlink Technical Manual (1966).
[10] F. Winkelmann, S. Selkowitz, Daylighting simulation in the DOE-2 building energy analysis program, Energy Build. 8 (1985) 271–286.
[11] C. Reinhart, Tutorial on the Use of Daysim Simulations for Sustainable Design, Institute for Research in Construction, National Research Council Canada, Ottawa, Canada, 2005.
[12] J. Hand, Strategies for Deploying Virtual Representations of the Built Environment: aka The ESP-r Cookbook, University of Strathclyde, Glasgow, UK, 2015.
[13] J. Mardaljevic, Daylighting simulation: validation, sky model and daylight coefficient, in: Ph.D. Thesis, De Montfort University, Leicester, UK, 2000.
[14] C. Reinhart, M. Andersen, Development and validation of a Radiance model for a translucent panel, Energy Build. 87 (2006) 890–904.
[15] C. Reinhart, P. Breton, Experimental validation of Autodesk® 3ds Max® Design 2009 and Daysim 3.0, Leukos 6 (2009) 7–35.

[16] D. Bourgeois, C. Reinhart, G. Ward, Standard daylight coefficient method for dynamic daylighting simulations, Build. Res. Inf. 36 (2008) 68–82.
[17] R. Perez, R. Seals, J. Michalsky, All-weather model for sky luminance distribution—preliminary configuration and validation, Sol. Energy 50 (1993) 235–245.
[18] G. Ward, R. Shakespeare, Rendering with Radiance: The Art and Science of Lighting Visualization, Morgan Kaufmann, San Francisco, 1998.
[19] S. Ranasinghe, R. Mistrick, A study of photosensor configuration and performance in a daylighted classroom space, J. Illum. Eng. Soc. N. Am. 32 (2003) 3–20.
[20] S. Kim, K. Song, Determining photosensor conditions of a daylight dimming control system using different double-skin envelope configuration, Indoor Built Environ. 16 (2007) 411–425.
[21] J. Mardaljevic, Validation of lighting simulation program under real sky conditions, Light. Res. Technol. 27 (1995) 181–188.
[22] Y. Yoon, Development of a fast and accurate annual daylight approach for complex window systems, in: Ph.D. Thesis, The Pennsylvania State University, Pensylvania, USA, 2006, pp. 60.
[23] P. Tregenza, L. Waters, Daylight coefficients, Light. Res. Technol. 15 (1983) 65–71.
[24] M. Rea, IESNA Handbook, 9th edition, The Illuminating Engineering Society of North America, NY, USA, 2002.
[25] R. Perez, P. Ineichen, R. Seals, J. Michalsky, R. Stewart, Modeling daylight availability and irradiance components from direct and global irradiance, Sol. Energy 44 (1990) 271–289.
[26] Y. Yoon, J. Lee, S. Kim, Development of computation algorithm for prediction of photosensor signals in daylight conditions, Build. Environ. 89 (2015) 229–243.
[27] W. Marion, K. Urban, User's Manual for TMY2s, NREL, 1995.
[28] P. Vik, Regression, ANOVA, and General Linear Model: A Statistics Primer, SAGE Pulbication, Inc., Londo, UK, 2013.
[29] J. Stapleton, Linear Statistical Models, 2nd edition, Wiley, New Jersey, USA, 2009.
[30] J. Neter, K. Kutner, W. Wasserman, C. Nachtsheim, Applied Linear Statistical Models, McGraw-Hill/Irwin, New York, USA, 1996.
[31] Campbell Scientific Inc, CR 23X Micro Logger Operator's Manual, Campbell Scientific, Inc., USA, 2000.
[32] LI-COR Inc, LI-COR Sensor Instruction Manual, LI-COR Inc., USA, 1991.
[33] J. Lee, Y. Yoon, Y. Baik, S. Kim, Analyses on human responses to illuminance variations for resident-friendly lighting environment in a small office, Indoor Built Environ. 22 (2013) 535–550.
[34] J. Lee, J. Moon, S. Kim, Analysis of occupants' visual perception to refine indoor lighting environment for office tasks, Energies 7 (2014) 4116–4139.